Structural and functional analysis of a potent human neutralizing antibody against enterovirus A71

Zhe Chen[1†], Linlin Bao[2†], Bin Zhu[3†], Hua Fu[1†], Shuangli Zhu[4], Tianjiao Ji[4], Ying Xue[1], Chuan Liu[5], Xurong Wang[6], Fengdi Li[2], Qi Lv[2], Feifei Qi[2], Pin Yu[2], Wei Deng[2], Wenbo Xu[4*], Chuan Qin[2*], Hongrong Liu[6*] & Qi Jin[1,7*]

[1]*MOH Key Laboratory of Systems Biology of Pathogens, Institute of Pathogen Biology, Chinese Academy of Medical Sciences & Peking Union Medical College, Beijing 100730, China;*
[2]*Beijing Key Laboratory for Animal Models of Emerging and Remerging Infectious Diseases, NHC Key Laboratory of Human Disease Comparative Medicine, Institute of Laboratory Animal Science, Chinese Academy of Medical Sciences and Comparative Medicine Center, Peking Union Medical College, Beijing 100021, China;*
[3]*School of Computer Science and Engineering, Hunan University of Science and Technology, Xiangtan 411201, China;*
[4]*National Institute for Viral Disease Control and Prevention, China CDC, Beijing 102206, China;*
[5]*Ministry of Education Key Laboratory of Protein Sciences, Beijing Advanced Innovation Center for Structural Biology, Tsinghua University, Beijing 100084, China;*
[6]*Key Laboratory for Matter Microstructure and Function of Hunan Province, Key Laboratory of Low-dimensional Quantum Structures and Quantum Control, School of Physics and Electronics, Hunan Normal University, Changsha 410081, China;*
[7]*Collaborative Innovation Center for Diagnosis and Treatment of Infectious Diseases, Hangzhou 310058, China*

Enterovirus A71 (EV-A71) causes major outbreaks of hand, foot, and mouth disease (HFMD) in many countries, most frequently affecting children, and a small proportion of cases may lead to death. Currently, no vaccine is available in most endemic regions, and no licenced treatments for EV-A71 infection are available. Here, we characterize a human monoclonal antibody (HuMAb), E1, by screening a Fab antibody phage library derived from patients who recovered from EV-A71 infection. E1 exhibits strong neutralizing activity against EV-A71 virus in cells. The cryo-electron microscopy (cryo-EM) structures of the EV-A71 virion in complex with E1 Fab fragments demonstrated that E1 recognized an epitope formed by residues in the BC and HI loops of VP1. In a mouse model, E1 effectively protected against lethal EV-A71 challenge in both prophylactic and therapeutic treatment. In particular, E1 significantly reduces virus titers and muscle damage. E1 might represent a potential adjunct to EV-A71 treatment.

enterovirus A71, antibody, mouse models, cryo-electron microscopy

INTRODUCTION

Enterovirus A71 (EV-A71) is a small, single-stranded, po-

sitive-sense RNA virus from the enterovirus genus in the family Picornaviridae. The viral capsid comprises 60 identical subunits (protomers), each of which contains a copy of the four structural viral proteins (VP1 to VP4) (Plevka et al., 2012). EV-A71 entry into susceptible cells requires coordinated interactions of the virus with compatible receptors. Several cellular receptors for EV-A71 have been identified:

scavenger receptor B2 (SCARB2), P-selectin glycoprotein ligand-1 (PSGL-1), and heparan sulfate (HS) (Nishimura et al., 2009; Tan et al., 2012; Yamayoshi et al., 2009). Each of the EV-A71 receptor interactions is critical for the successful entry of EV-A71 into host cells and the establishment of infection.

EV-A71 causes major outbreaks of hand, foot, and mouth disease (HFMD), most frequently affecting children. During outbreaks, thousands of children can develop HFMD, and although most have self-limiting illness, a small proportion can rapidly develop neurological and systemic complications that can be fatal (Ooi et al., 2010). EV-A71 was first isolated from a child with encephalitis in California in 1969 (Schmidt et al., 1974). Large outbreaks have recently occurred in Singapore, India, Thailand, Hong Kong (China), Malaysia and Brunei (Bible et al., 2007). The 2018 outbreak in Vietnam was associated with over 50,000 clinical cases and at least six deaths (Nhan et al., 2018).

Although two inactivated vaccines (EV-A71 C4) have approved by Chinese Food and Drug Administration, there are no vaccines currently available in most endemic regions and no licenced treatments for EV-A71 infection. New preventative and therapeutic strategies are urgently needed to counter this threat. Neutralizing antibodies (nAbs) have been considered promising prophylactic and therapeutic interventions against viral diseases. In particular, human-derived nAbs are most suitable for use in clinical treatment, as they have a lower risk.

In the present study, we isolated E1, a fully human neutralizing antibody against EV-A71, from the peripheral B cells of a convalescent donor who survived EV-A71 infection. Human mAb E1 showed potent neutralizing activity against EV-A71. Its efficacy as both a prophylactic and therapeutic antibody was evaluated by lethal challenge with EV-A71 in a mouse model. The cryo-EM structures of the EV-A71 virion in complex with E1 Fab fragments demonstrated that E1 recognized an epitope formed by residues in the BC and HI loop of VP1. Thus, E1 shows promise as a candidate therapeutic for the treatment of human EV-A71 infection.

RESULTS

Characterization of the anti-EV-A71 neutralizing mAbs E1

Fab phage display libraries containing 1×10^8 independent clones were established. After three rounds of panning, one Fab antibody that strongly reacted with antigens, E1, was initially isolated and converted into full-length human IgG1, with light chain $V_\lambda 3$ and heavy chain $V_H 1$. The neutralization activity of E1 was tested against five EV-A71 strains, including subgenotypes A, B5, C4a, and C4b (Table 1). EV-A71 strain GD10 (C4a), SD07-523 (C4a), SH02-17

Table 1 Neutralization activity of E1 on a panel of EV-A71[a]

Strain	Subgenotypes	Neutralization concentration ($\mu g\ mL^{-1}$)
GD10	C4a	0.78
SD07-523	C4a	0.39
SH02-17	C4b	0.195
BrCr	A	–
BJ18-22	B5	0.39

a) Neutralization concentration was determined as the lowest antibody concentration required to fully prevent cytopathic effect (CPE).

(C4b) and BJ18-22 (B5) were sensitive to neutralization by E1, whereas strains BrCr (A) was resistant. Biolayer interferometry analysis showed that the affinities of the antibodies E1 to the EV-A71 dissociation constant values were 2.00×10^{-7} mol L^{-1} (Figure S1B in Supporting Information). Then we investigated whether E1 could interfere with EV-A71 binding to receptor Heparan sulfate glycosaminoglycan by pulldown assays. E1 could reduce the amount of virus pulled down in a dose-dependent manner when 1 μg and 10 μg of E1 were applied (Figure S2 in Supporting Information). In addition, we generated three EV-A71 mutants that can escape the neutralization of E1. These mutants revealed that all three mutant viruses had a single amino acid change at the position of E98K within the VP1 BC-loop.

Prophylactic efficacy of E1 in mice

To explore the prophylactic efficacy of E1, mice were inoculated intravenously with the antibody at 10 mg kg^{-1} (designated E1-pre 24 h). The mice were then challenged with EV-A71 24 h later. A control group was infected at the same time and inoculated intravenously with naive human IgG as a control IgG. The clinical signs, body weight changes and survival of the mice were monitored every day. The control mice developed paralysis at 4 d post-infection (dpi), and all of them died within 10 dpi. Prophylactic administration of E1 got the survival rate of infected mice to 100% (Figure 1A).

Therapeutic efficacy of E1 in mice

To further study the treatment efficacy of E1, the mice were inoculated intravenously with the antibody at 10 mg kg^{-1} 2 h (designated E1-2h) and 12 h (designated E1-12h) post-infection with EV-A71. The mice infected with EV-A71 and treated with E1 had a survival rate of 100% (Figure 1A). The clinical scores of infected mice subjected to prophylaxis and treatment with E1 were systematically evaluated. Mice subjected to prophylaxis with E1 and treatment with E1-2h showed no obvious clinical symptoms, and mice subjected to treatment
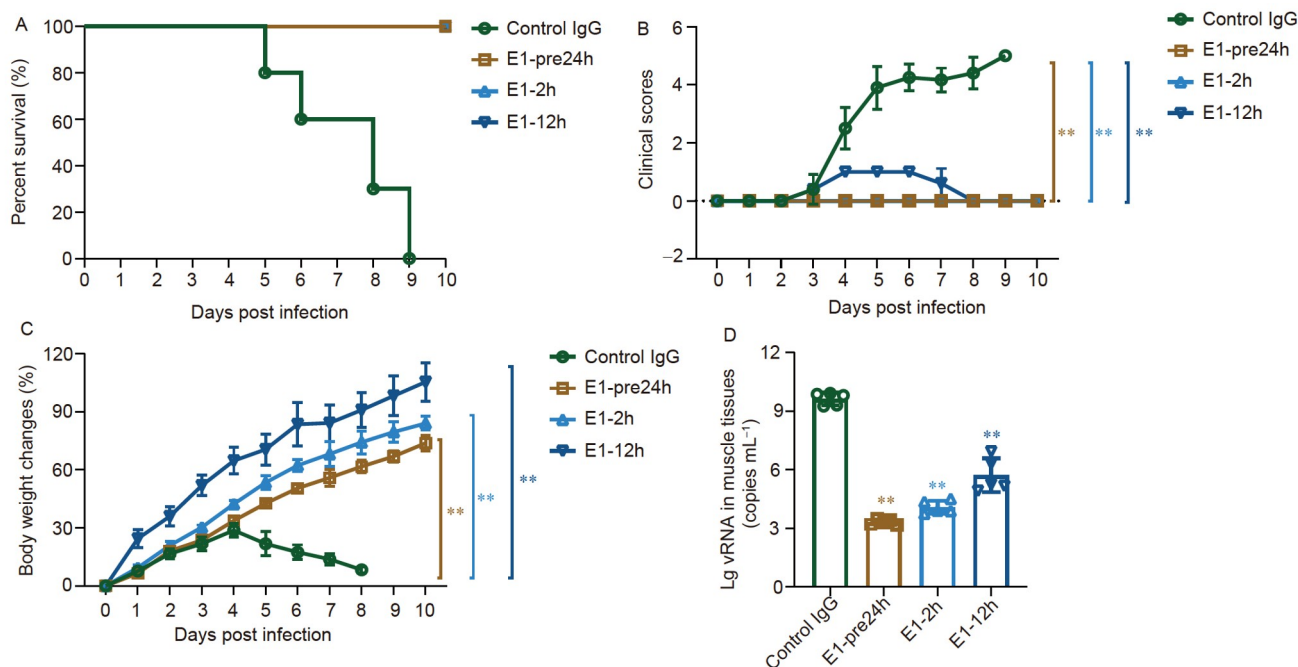
Figure 1 Prophylactic and therapeutic efficacy of E1 in BALB/c mice. E1 prophylaxis and treatment reduced the mortality of EV-A71-infected mice. A, Survival rates of the EV-A71 infected mice subjected to prophylaxis with E1 (10 mg kg^{-1}) at 24 h pre-infection and treatment with E1 (10 mg kg^{-1}) at 2 h or 12 h post-infection were recorded at 10 dpi (n=10 per group). B, The clinical scores of infected mice subjected to prophylaxis with E1 (10 mg kg^{-1}) at 24 h pre-infection and treatment with E1 (10 mg kg^{-1}) at 2 h or 12 h post-infection were systematically evaluated (n=10 per group). **, $P<0.01$. C, Weight change rates of the EV-A71 infected mice subjected to prophylaxis with E1 (10 mg kg^{-1}) at 24 h pre-infection and treatment with E1 (10 mg kg^{-1}) at 2 h or 12 h post-infection were recorded at 10 dpi (n=10 per group). **, $P<0.01$. D, The infected mice were subjected to prophylaxis and treatment with E1 (10 mg kg^{-1}) at 2 h or 12 h post-infection. The muscle tissues were sampled at 5 dpi (n=5). The viral copy numbers were determined by qRT-PCR (**, $P<0.01$).

with E1-12h showed signs of weakness (Figure 1B).

In addition to the control IgG group, the weight of the mice continued to decline from 4 dpi to the end, and the weight of the mice in the prevention group and the treatment group after infection rose continuously (Figure 1C).

E1 treatment reduces viral replication and muscle damage

Consistent with these results, compared with that of the IgG control, virus replication in the muscle of mice subjected to prophylaxis and treatment with E1 was inhibited by $10^{3.90}$- to $10^{6.31}$-fold at 5 dpi, as detected by qRT-PCR (Figure 1D). In the control IgG group, serious muscle necrosis appeared at 5 dpi and led to paralysis of the mice (Figure 2A), while the E1 prophylactic group had no obvious muscle damage, and the E1 treatment group a certain degree improved muscle damage caused by EV-A71 infection (Figure 2B–D). In addition, the muscle tissues lesions of control IgG group showed a large amount of positive viral particles (Figure 3A), and no remarkable virus distribution were observed the E1 treatment group via immunohistochemistry (IHC) (Figure 3B–D).

Cryo-EM reconstruction of E1 bound to EV-A71

We harvested two kinds of virons during cell culture: the

mature virions with the infectious RNA genome and the immature empty particles. Since, the mature virus and the empty particle are similar in surface structure and antigenicity, the higher amount of empty virus was used for cryo-EM reconstruction (Figure S3 in Supporting Information). EV-A71 has an icosahedral capsid formed by 60 identical units, so this symmetry was first used to build the structure of the Fab and the virus complex. The whole complex was resolved to 4.89 Å (Figure 4C). From the map, extra densities corresponding to antibodies were observed at the 5-fold vertices of the virus shell (Figure 4A). As a result of icosahedral symmetry averaging, there should be densities for five Fab molecules around the 5-fold axis. However, it was identified that only a single Fab structure can be fitted in the density, and other Fabs cannot be fitted in the same 5-fold density due to steric hindrance. Therefore, every pentamer and its binding Fab were extracted as a subunit that was resolved with C1 symmetry.

The cryo-EM structure of the extracted subunit was determined to a resolution of 4.33 Å (Figure 4B and D). Most side-chain densities of the virus capsid were shown clearly, with the exception of some peripheral regions contacting Fab. Fab was resolved at a lower resolution due to its flexibility, and only the backbone could be traced. Although we were unable to build a *de novo* atomic model at the current resolution, the cryo-EM map was of sufficient
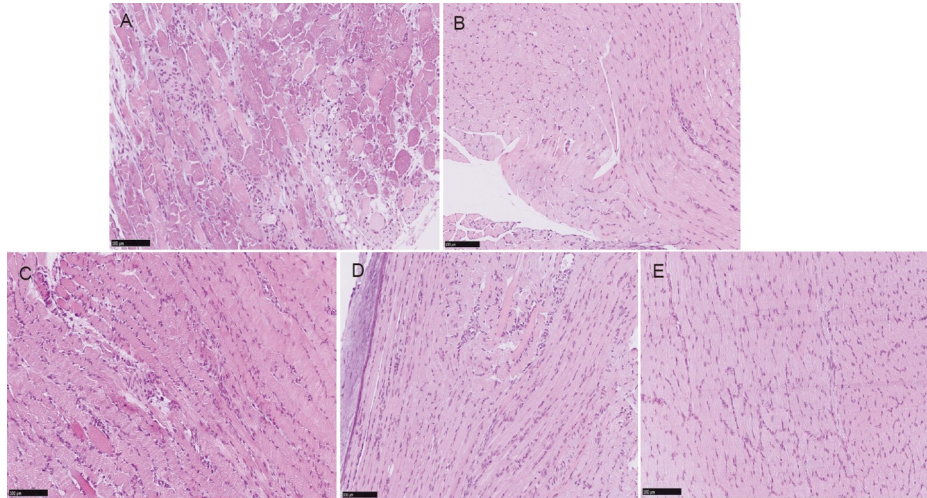
Figure 2   Histopathology. E1 reduced the virus distribution and pathological damage. The infected mice were subjected to prophylaxis with E1 (10 mg kg^{-1}) at 24 h pre-infection and treatment with E1 at a dose of 10 mg kg^{-1} at 2 h or 12 h post-infection. The muscle tissues were sampled at 5 dpi for pathological analysis. Pathological changes were observed after H&E staining. A, Control IgG group: skeletal muscle deformation and necrosis, interstitial inflammatory cell infiltration. B, E1-pre-24h group: no obvious muscle damage. C, E1-2h group: focal myofibrillary degeneration with a small amount of inflammatory cell infiltration in the interstitium. D, E1-12h group. Focal myofibrillary degeneration with a small amount of inflammatory cell infiltration in the interstitium. E, Blank mice group. Magnification: 100×.
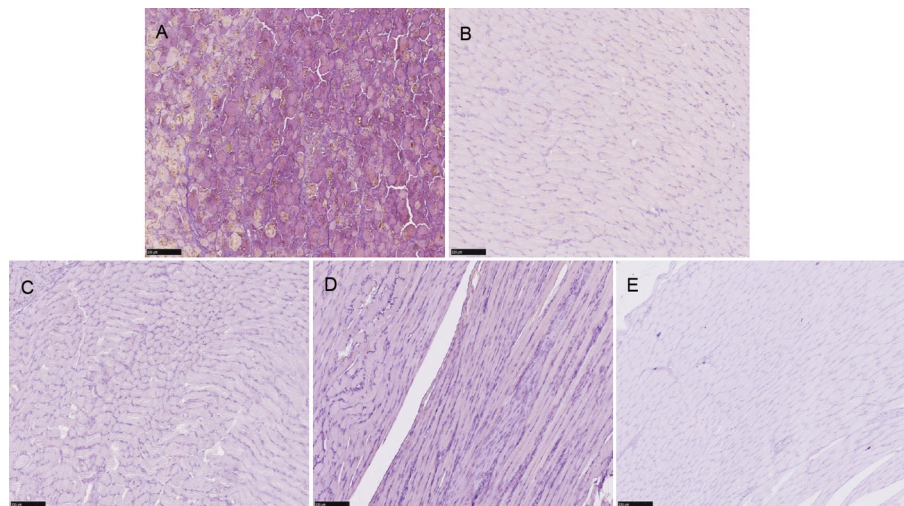

Figure 3   Immunohistochemistry. E1 reduced the virus distribution and pathological damage. The infected mice were subjected to prophylaxis with E1 (10 mg kg^{-1}) at 24 h pre-infection and treatment with E1 at a dose of 10 mg kg^{-1} at 2 h or 12 h post-infection. The muscle tissues were sampled at 5 dpi for pathological analysis. Pathological changes were observed after H&E staining, and the viral antigens were detected by IHC against the EV-A71. A, Control IgG group. B, E1-pre-24h group. C, E1-2h group. D, E1-12h group. (*n*=5 per group). E, Blank mice group. Magnification: 100×.

quality to unambiguously fit homologous structures for Fab and the virus pentamer (Figure 5A and B). The three-dimensional (3D) map revealed that Fabs were located at apical surfaces of the pentavalent capsomers (Figure 5A). Several obvious density connections between the Fab variable domain and the virus capsid proteins are shown in the cryo-EM map (Figure 5C and D). When increasing the contour level, two connections did not disappear until a portion of the density for the capsid was missing from the cryo-EM map. The two connecting densities indicate the most likely regions where Fabs bound to the capsid. Following docking of the structure of the complex, the VP1 BC loop (residues 96–102) and HI loop (residues 239–247) were identified to be involved in the interaction between Fab and the virus (Figure 5C and D).

DISCUSSION

Recently, human monoclonal antibody development has become more common in the field of infectious diseases, particularly in the context of emerging infectious disease outbreaks, such as SARS-CoV-2, Ebola and Zika (Robbiani et al., 2017; Wec et al., 2019; Zost et al., 2020). Previous
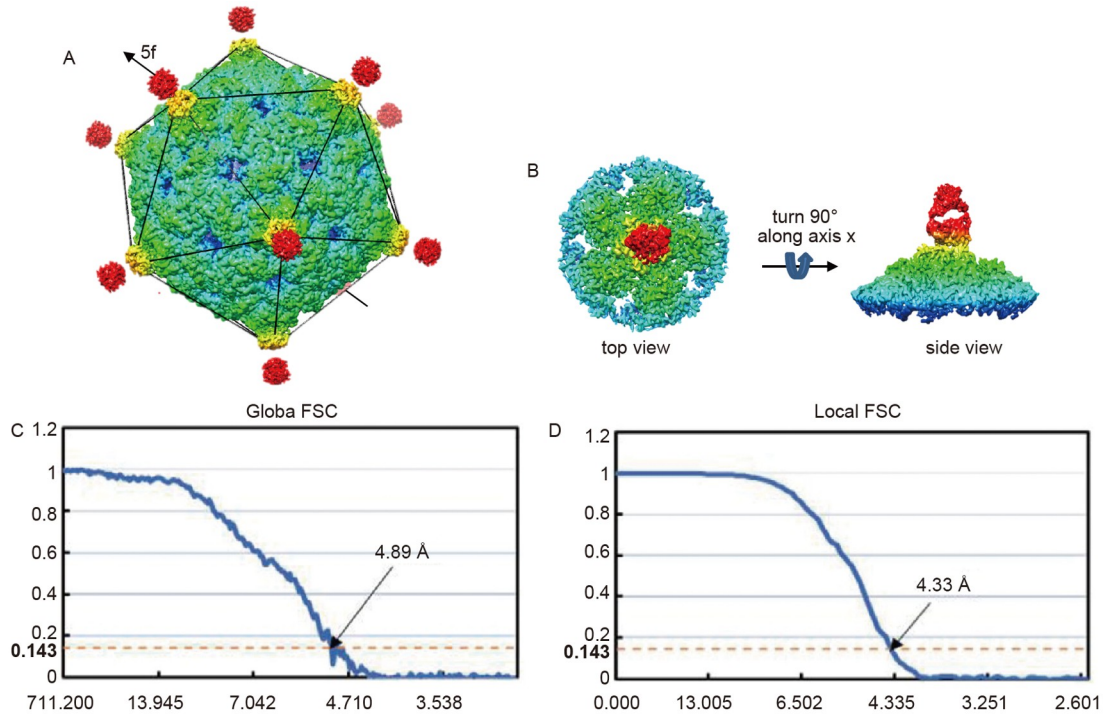
Figure 4   The cryo-EM structure of the EV-A71-fab complex. The structure of the antibody complexed with the whole virus and the virus pentamer were resolved respectively. A, The global structure of the complex resolved with icosahedral symmetry. B, The structure of the virus pentamer and Fab reconstructed with C1 symmetry. C, Gold standard Fourier shell correlation (FSC) curves for reconstruction of the global structure. D, The virus pentamer complexed with Fab.
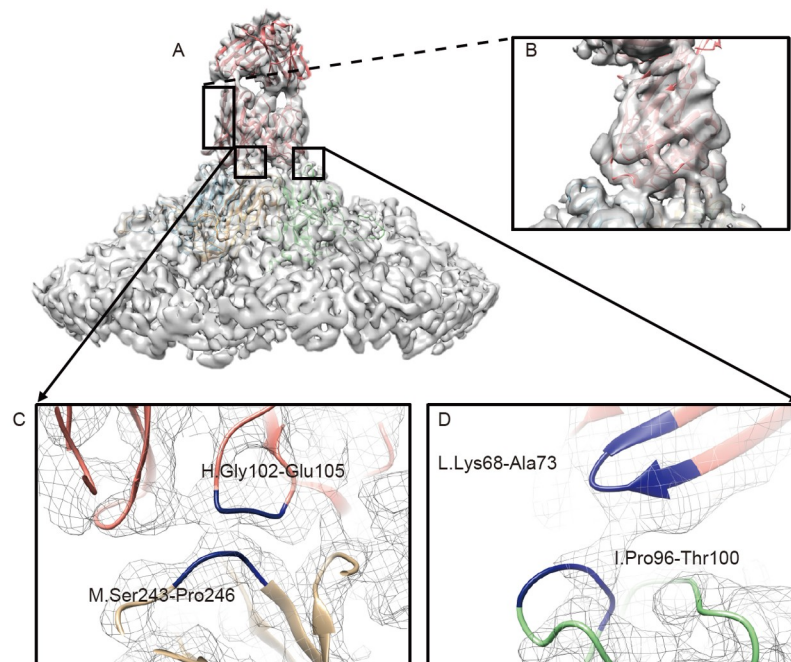

Figure 5   Overall density map of local reconstructed EV-A71 pentamer with Fab. Homology model was fitted into the density of the cryo-EM reconstruction and the interaction regions have been identified. A, Fit of the homology model (ribbon) into the cryo-EM density map (grey mash). B, Zoomed-in view shows that three β strands (a-b, c-d, e-f) fit well with our density map and make our structure very convincing. C and D, Two enlarged views of the boxed region show interactions between Fab and the VP1 HI loop (C) and between Fab and the VP1 BC loop (D). Interaction regions are colored in blue.

antibody research on EV-A71 has mostly used murine antibodies (Kiener et al., 2014; Ku et al., 2015; Shingler et al., 2015), except for two antibodies: 38-1-10A and 38-3-11A

(Huang et al., 2020). Reports about human antibodies against EV-A71 are very rare, and high-quality human antibodies with high specificity, avidity and neutralizing activity might

be a viable treatment option for EV-A71 infection in humans. In the present study, we isolated E1, a fully human neutralizing antibody against EV-A71, from the peripheral B cells of a convalescent donor who survived EV-A71 infection. Human mAb E1 showed potent neutralizing activity against EV-A71.

BALB/c mice are highly susceptible to EV-A71 infection; therefore, we selected BALB/c mice to assess the prophylactic and therapeutic efficacy of E1. All model animals developed serious HFMD disease and suffered from noticeable body weight losses. Furthermore, the control mice developed paralysis at 4 dpi, and all of them died within 10 dpi. Treatment with E1, both pre- and post-exposure to viral infection, improved clinical and pathological features in the infected mice. Viral replication and titers are important during the course of disease development. Low viral titers were detected in E1-treated animals at 5 dpi in both prophylactic and therapeutic experiments. Furthermore, in the control IgG group, serious muscle necrosis appeared at 5 dpi and led to paralysis of the mice, while the E1 prophylactic group and treatment group had no obvious muscle damage caused by EV-A71 infection. The results of therapeutic experiments showed that E1 will be beneficial as a new therapeutic strategy for EV-A71.

Previously, EV-A71 neutralizing antibody D5 fully inhibited EV-A71 (G081) replication at 0.625 μg mL^{-1} and treatment fully protected mice with 5×10^5 tissue culture infectious dosage (TCID$_{50}$) of EV-A71 infection. It may preoccupy the SCARB2-binding site with targeting GH loop of VP3. Mabs 5H7 is able to neutralize EV-A71 before virus attachment and protect 100% of two-week-old AG129 mice from lethal challenge with an EV-A71 B4 strain by inhibiting virus binding to SCARB2 receptor (Ku et al., 2015; Jia et al., 2017; Ye et al., 2016). To understand the neutralization mechanisms of E1, we used cryo-EM reconstruction of E1 bound to EV-A71. The 5-fold vertices of the EV-A71 capsid are important for eliciting neutralizing antibody responses and mediating receptor binding (Oberste et al., 1999). Under some conditions, binding of the antibody to the 5-fold vertex of the virus will make the antibody incompatible with icosahedral symmetry, which is a challenge for high-resolution structure determination of the antibody with the virus as a whole (Lee et al., 2013). In the present study, we improved the resolution by determining the structure of EV-A71 and the human monoclonal antibody fragment complex at 4.33 Å resolution with a local reconstruction method (Figure 4B and D), which provided the necessary information to interpret the structure and understand the interaction of the virus and Fab. The cryo-EM map showed that a single Fab stands on three capsomers of the 5-fold plateau and almost covers its top surface. Further analysis of the complex structure revealed that the BC loop and HI loop of VP1 were in close contact with E1, respectively (Figure 5C and D; Table S1 in Sup-

porting Information). The VP1 HI loop plays a vital role in the binding of EV-A71 to the cellular receptor PSGL-1. Two positive residues (VP1-244 and VP1-242) within the HI loop are responsible for the binding of the negatively charged sulfated tyrosines in the N-terminus of PSGL-1 (Nishimura et al., 2010; Nishimura et al., 2013). Interestingly, it was clearly shown that densities at two locations of the HI loop are connected to Fab. Particularly at one site, the linking persisted when we increased the contour level (data not shown). In addition to PSGL-1, the positive sites of the HI loop are also critical for binding to cell surface HS, which is known to serve as an attachment receptor for EV-A71 (Tan et al., 2012). According to these data, Fab may interfere with the interaction of PSGL-1 and HS with EV-A71, impairing attachment and entry of the virus into the target cell.

BC loop has been reported to be necessary for the virus binding to its cell receptor by a previous study which identified that amino acid mutations within BC loop and near the fivefold axis are involved in the resistance of EV-A71 to a compound blocking EV-A71 interaction with PSGL-1 and HS (Ranganathan et al., 2002). Inconsistent with their report, the cryo-EM structure of our study showed that Fab interacts with two adjacent BC loops. These studies suggest that the BC loop is necessary for the binding of the virus to the cell receptor. The interaction regions between E1 and the two adjacent BC loops may serve as two supporting points that will favour the contact between the HI loop and the antibody. A notable residue from DE loop, VP1-145, has been demonstrated to modulate the interaction of VP1-244 and PSGL-1 by controlling the orientation of the lysine side chain of VP1-244 (Nishimura et al., 2013). No close contact between the region around VP1-145 and Fab was observed in the present study, indicating that E1 probably does not interact with the virus at this site directly.

In summary, we identified and characterized HuMAb E1, which possess potent neutralizing activity against EV-A71 *in vitro*. E1 recognized the BC (residues 96–102) and HI loops (residues 239–247) of VP1 and provided strong defences against challenge with lethal doses of EV-A71 in mice. Thus, we proposed that E1 should be considered a promising candidate for EV-A71 treatment.

MATERIALS AND METHODS

Ethics statement

This study was reviewed and approved by the Ethics Committee of the Institute of Pathogen Biology, Chinese Academy of Medical Sciences & Peking Union Medical College. Peripheral blood samples from HFMD patients were collected at Linyi Peoples Hospital in Shandong Province, China. Written informed consent from their parents was obtained for the use of peripheral blood samples.

All animal experiments were approved by the Institutional Animal Care and Use Committee (IACUC) of the Institute of Laboratory Animal Science (ILAS), Peking Union Medical College (BLL-17-006), and performed following Chinese national guidelines for the care of laboratory animals. All procedures were performed to minimize suffering. The animals were housed in adjoining individual primate cages to facilitate social interactions, under controlled conditions of humidity, temperature and light (12 h light/12 h dark cycle). Food and water were available *ad libitum*. The animals were monitored twice daily (pre- and post-challenge). End-point criteria, as specified by the scoring parameters approved by the ILAS IACUC, were used to determine when animals should be humanely euthanized. Animals were euthanized by exsanguination under deep anaesthesia. All experiments with live EV-A71 were carried out following the standard operating procedures of the biosafety level 2 facilities.

Cells and viruses

Rhabdomyosarcoma (RD) cells (ATCC) were maintained in Dulbecco's modified Eagle's medium (DMEM; Gibco, USA) containing 10% fetal bovine serum (FBS; Gibco). EV-A71 strain GD10 (C4a), (GenBank accession NO. KJ004559.1) SD07-523 (C4a), SH02-17 (C4b), BJ18-22 (B5) and BrCr (A) was used. Virus titer determination and purification were performed to determine the median endpoint of the $TCID_{50}$. Serially diluted virus samples (from 10^{-2} to 10^{-9}) were added to RD cells in 96-well plates (Costar, USA), and eight wells were used at each dilution. The 96-well plates were incubated for 7 d at 37°C, and the $TCID_{50}$ values were measured by determining the cytopathic effect (CPE). The $TCID_{50}$ values were calculated by the Reed-Muench method. The virus was inactivated with formalin for 5 d at 44°C, purified by precipitation with 7% polyethyleneglycol 8000 and then centrifuged onto a 30% sucrose cushion at $25,000 \times g$ for 3 h.

Phage library construction

Peripheral blood mononuclear cells (PBMCs) were isolated from the peripheral blood of recovered patients 3–4 weeks after hospitalization. RNA was then extracted and purified from the lymphocytes using the RNeasy kit (Qiagen, Germany) according to the manufacturer's protocol. cDNA was transcribed using total RNA as a template, ThermoScript Reverse Transcriptase (Invitrogen, USA) as the enzyme, and oligo dT as the primer. The heavy and light chain genes were amplified from the cDNA using PCR and sequentially cloned into the phagemid vector pComb3H (kindly provided by the Scripps Research Institute, USA). The anti-EV-A71 phage antibody library was constructed using previously described primers and methods (Barbas et al., 1991).

Selection of EV-A71 specific Fabs

The antibody library was screened by panning with purified EV-A71 virions. After three rounds of panning, crude Fab antibody preparations were tested by indirect enzyme-linked immune sorbent analysis (ELISA) using 96-well plates coated with purified EV-A71 virions at a concentration of 50 ng per well. Horseradish peroxidase (HRP)-conjugated anti-human Fab was used as the secondary antibody. Human Fab mAbs were purified on an anti-Fab affinity chromatography column for further characterization and functional analysis. The purity of the human Fab mAbs was confirmed using SDS-PAGE analysis.

IgG1 expression and purification

Human IgG1 mAbs were expressed and purified as described previously (Rader et al., 2002). Briefly, fully human IgG1 antibodies were constructed by cloning the heavy and light chain variable regions of EV-A71 specific antibodies into PIGG vectors (provided by the Scripps Research Institute) for IgG1 heavy and light chain expression. IgG1 samples were produced from the PIGG vector by transiently transfecting human 293T cells using Lipofectamine 2000 (Invitrogen). The collected medium was purified by affinity chromatography using a recombinant Protein AHiTrap column (GE Healthcare, USA). The purity of IgG1 was confirmed using SDS-PAGE and ELISA.

Neutralization assay

Briefly, human IgG1 mAbs were subjected to serial 2-fold dilution using DMEM containing 2% FBS, and then 50 μL of 100 $TCID_{50}$ EV-A71 viral samples combined with mAbs were incubated at 37°C for 1 h. The virus and mAb mixtures (total 100 μL) were inoculated onto 70%-confluent RD cells in a 96-well plate and monitored for the development of the characteristic CPE for 4 d. The highest dilution of mAbs that inhibited virus growth was considered the neutralization antibody titer and determined after incubation at 37°C for 4 d.

Biolayer interferometry assay

Antibody binding to EV-A71 was analyzed by biolayer interferometry on an Octet Red 96 system (ForteBio, USA) in PBS buffer at room temperature. The inactivated EV-A71 (GD10) was labeled with biotin using an EZ-Link sulfo-NHSLC-LC-biotin kit (Thermo Fisher Scientific, USA). After a brief rinse in kinetics buffer, the streptavidin (SA) biosensor tips were dipped into 200 μg mL^{-1} of EV-A71 biotin solution for 10 min. Following a rinse in kinetics buffer, the EV-A71 immobilized biosensor tips were allowed to associate with antibody at different concentrations (2,000,

400 and 80 µg mL^{-1}) for 25 min and then dissociate in kinetics buffer for 10 min. The EV-A71 bound biosensor was also allowed to associate with kinetics buffer alone (without antibody) to serve as a loading control. In addition, an empty sensor tip (without EV-A71 loading) was allowed to associate with 2,000, 400 and 80 µg mL^{-1} of antibody to assess nonspecific antibody binding. Data were processed using Octet data analysis (v6.4) software (ForteBio), and affinity values were calculated by steady-state analysis.

Pulldown assays

For heparin pulldown assays, different amounts of mAb were mixed with 1×10^6 TCID$_{50}$ of EV-A71 GD10 in 400 µL DMEM containing 2% FBS, and the mixtures were incubated at 37°C for 1 h, followed by addition of 20 µL of heparin-agarose (Sigma-Aldrich, USA) and subsequent incubation at 4°C for 2 h. The antibody-virus-bead mixtures were subjected to centrifugation at 500×*g* for 3 min. The supernatants were discarded, and the beads were washed three times. Virus-bound beads were analyzed by SDS-PAGE and Western blotting with a rabbit anti-EV-A71 polyclonal antibody (Ku et al., 2015).

Generation and sequencing of E1-escaping mutants

Briefly, E1 (400 µg mL^{-1}) was mixed with 1×10^5 TCID$_{50}$ of EV-A71 GD10 virus, and the mixture was incubated at 37°C for 2 h. The virus/antibody mixtures were added to 70%-confluent RD cells, followed by incubation for 3 d at 37°C. The cultures were harvested and subjected to three freeze-thaw cycles. If no CPE was observed, the supernatants were harvested, and repeated until CPE was observed. Then, the resulting E1-resistant viruses were plaque purified on RD cells. The E1-resistant viruses were used for RNA extraction and purification by RNA isolation kit (Qiagen). The cDNA was generated from the total RNA as template using Thermoscript reverse transcriptase (Invitrogen) with oligo dT as primer. The P1 region was amplified and subsequently verified by sequencing.

Prophylaxis and therapy in mouse models

Ten- or eleven-day-old specific pathogen-free BALB/c mice were provided by the Institute of Laboratory Animal Science, Peking Union Medical College. All of the animal protocols were approved by the institutional animal care and use committee.

To measure the prophylactic efficacy, mice (10 mice per group) were inoculated intravenously with 10 mg kg^{-1} purified mAb E1 24 h before the mice were challenged intraperitoneally with 10^7 PFU mL^{-1} (lethal dose) of GD10 EV-A71 virus. Another ten mice immunized with an irrele-vant human IgG were also infected as controls. Mice were observed daily for signs of disease and mortality for up to 10 d. For therapy against EV-A71, the mice (also 10 mice per group) were first infected with 10^7 PFU mL^{-1} EV-A71, then 2 or 12 h later, they were injected with 10 mg kg^{-1} purified mAb E1 and observed daily for signs of disease and mortality for up to 10 d. Control human IgG-treated mice were infected in the same way and monitored every day.

Histopathology

For each experimental group, mice were subjected to pathologic examination. After euthanasia, the muscle tissues (skeletal muscle of the thigh of the left hind leg) were immediately immersion-fixed in 10% buffered formalin for 48 h. The tissues were bisected, embedded in paraffin, and stained with haematoxylin and eosin (H&E).

Immunohistochemistry

For IHC staining to identify the expression of the EV-A71 antigen, dehydrated paraffin sections (3–4 µm in thickness) were treated with an antigen retrieval kit (Boster, Wuhan, China) for 1 min at 37°C and quenched for endogenous peroxidases in 3% H$_2$O$_2$ in methanol for 10 min. After blocking in 1% normal goat serum for 1 h at room temperature, the sections were stained with the rabbit polyclonal antibody to EV-A71 (1:500 dilution, GeneTex, USA) at 4°C overnight, followed by incubation with an HRP-labeled goat anti-rabbit IgG (Beijing ZSGB Biotechnology, China) for 1 h. Finally, the sections were visualized by incubation with 3,3′-diaminobenzidine tetrahydrochloride (DAB) and viewed using an Olympus microscope (Olympus, Japan).

Viral load study

The skeletal muscle of the thigh of the right hind leg was obtained from 5 mice of each group. RNA was extracted from 100 µL of each sample using the RNeasy Mini Kit (Qiagen). A total of 5 µL of RNA was added to a 25 µL reaction for one-step amplification (QuantiTect Probe RT-PCR Kit, Qiagen) and the amplification condition were as follows: 50°C for 10 min, 95°C for 10 min, followed by 40 cycles of 95°C for 15 s, and then 60°C for 45 s. The primers and probe sequences sets for VP1 genes of EV-A71 viruses: forward primer 5′-AGATAGAGTGGCAGATGTAAT-3′, reverse primer 5′-TTGATGATGCTCCAATCTCAG-3′. The probe sequence was 5′-FAM-CTCTACCAGCACACA-CAGGCCAGAAC-BQH1-3′.

Cryo-EM sample purification and preparation

The culture was harvested 3 d post-infection and processed

by three cycles of freezing and thawing. The lysate was centrifuged at 3,000×*g* to remove the cellular debris. The resulting supernatant was inactivated by treatment with β-propiolactone and filtered through a 0.22 μm pore-size Millipore filter. After ultracentrifugation on a 20% sucrose cushion (SW28 Ti rotor, 31,000×*g*, 4°C, 3 h), the pellets were resuspended in PBS (pH 7.4) and loaded on a 10%–50% sucrose gradient (SW60 Ti rotor, 25,000×*g*, 4°C, 2.5 h) in a Beckman centrifuge. Fractions containing the virus particles were collected and pelleted by ultracentrifugation through a 20% sucrose cushion. Then, the virus was re-suspended in PBS (pH 7.4) and concentrated to 1.0 mg mL^{-1}. The fraction of purified empty virus was mixed with the Fab fragment at a molar ratio of 240:1 (Fab:virus), providing an excess of four antibody molecules per possible binding site. After incubation on ice for 30 min, 3.5 μL of the mixture was applied to glow-discharged 200 mesh Quantifoil Holey Carbon Copper Grids 1.2/1.3 with a thin layer of continuous carbon film using FEI Vitrobot. The grids were blotted and plunged into liquid ethane cooled by liquid nitrogen for freezing.

Cryo-EM imaging, data collection and reconstruction

The specimen was examined under low-dose conditions with a TecnaiArctica 200 kV electron microscope. Micrographs were recorded on a Falcon II direct electron detector at a magnification of 78000X, corresponding to a pixel size of 1.27 Å. Movie frames were recorded with a total exposure time of 1.2 s using a total dose of 50 e/Å^2. Motion was corrected using MotionCorr (Li et al., 2013), and contrast transfer function (CTF) values were estimated with CTFFIND4.1 (Rohou and Grigorieff, 2015). The program e2boxer.py was used to manually pick particles that were extracted with a box size of 400 pixels (Tang et al., 2007). Conventional 3D structure refinement implemented in relion3.0 (Scheres, 2012) was used to refine the high-resolution EV-A71 antibody structure with imposed icosahedral symmetry I2. The word "antibody" in the particle image refers to antibody particles. We boxed those antibody particles by a previously reported method (Briggs et al., 2005; Ilca et al., 2015) according to the orientation of icosahedral symmetry to generate 60 orientations, among which five redundant orientations related to the same antibody particles with the same location and different rot angles were assigned into one group. One particle image could generate 12 antibody particle images, and all antibody particle-containing antibodies were treated as individual single particles. In total, 473,436 antibody particles were boxed from 39,453 image particles. Because the antibody bound to the monomers of pentamer is solid, symmetry mismatch reconstruction was performed to reconstruct the structure of the antibody (Chen et al., 2020). First, one of fivefold symmetry orientations of

each antibody particle was randomly selected to generate an initial model. Classfication 2D is run in relion to remove those pentamers without antibody, and then a projected template-match method that is similar to Frealign is used to search the best orientation in fivefold symmetry orientations without Classfication 3D. And the best orientation was selected to reconstruct the new map without symmetry. A diagram exhibits the cryo-EM data processing procedure (Figure S2 in Supporting Information). The resolution of antibody-pentamer was determined according to gold-standard Fourier shell correlation curve (FSC) at the 0.143 criterion.

Model building

The crystal structure of the virus pentamer (PDB ID:4rqp) was used as a reference to build the initial model by fitting the structure as a rigid body into our 4.3 Å-resolution cryo-EM map. A homology model for our Fab was generated through the SWISS-MODEL website using structures of 5aze.1 as a template. 5aze.1 has high sequence similarity to our Fab (92.82% sequence identity). Then, the homologous structure of our Fab was docked in the cryo-EM map in Chimera. The models were refined by using PHENIX and were adjusted manually in COOT (Emsley et al., 2010).

Statistical analysis

The virus titer was evaluated independently for each of the infected marmosets. All results are presented as the mean ±SD. Statistical analysis was performed by using SSPS10.0. Differences with *P*<0.05 were considered statistically significant.

Accession numbers

Local Cryo-EM density map has been deposited in the Electron Microscopy Data Bank (EMDB) and are available under accession number EMD-31392.

References

Barbas, C.F. 3rd, Kang, A.S., Lerner, R.A., and Benkovic, S.J. (1991). Assembly of combinatorial antibody libraries on phage surfaces: the

gene III site. Proc Natl Acad Sci USA 88, 7978–7982.

Bible, J.M., Pantelidis, P., Chan, P.K.S., and Tong, C.Y.W. (2007). Genetic evolution of enterovirus 71: epidemiological and pathological implications. Rev Med Virol 17, 371–379.

Briggs, J.A.G., Huiskonen, J.T., Fernando, K.V., Gilbert, R.J.C., Scotti, P., Butcher, S.J., and Fuller, S.D. (2005). Classification and three-dimensional reconstruction of unevenly distributed or symmetry mismatched features of icosahedral particles. J Struct Biol 150, 332–339.

Chen, W., Xiao, H., Wang, X., Song, S., Han, Z., Li, X., Yang, F., Wang, L., Song, J., Liu, H., et al. (2020). Structural changes of a bacteriophage upon DNA packaging and maturation. Protein Cell 11, 374–379.

Emsley, P., Lohkamp, B., Scott, W.G., and Cowtan, K. (2010). Features and development of *Coot*. Acta Crystlogr D Biol Crystlogr 66, 486–501.

Huang, K.Y.A., Zhou, D., Fry, E.E., Kotecha, A., Huang, P.N., Yang, S.L., Tsao, K.C., Huang, Y.C., Lin, T.Y., Ren, J., et al. (2020). Structural and functional analysis of protective antibodies targeting the threefold plateau of enterovirus 71. Nat Commun 11, 5253.

Ilca, S.L., Kotecha, A., Sun, X., Poranen, M.M., Stuart, D.I., and Huiskonen, J.T. (2015). Localized reconstruction of subunits from electron cryomicroscopy images of macromolecular complexes. Nat Commun 6, 8843.

Jia, Q., Ng, Q., Chin, W., Meng, T., Chow, V.T.K., Wang, C.I., Kwang, J., and He, F. (2017). Effective *in vivo* therapeutic IgG antibody against VP3 of enterovirus 71 with receptor-competing activity. Sci Rep 7, 46402.

Kiener, T.K., Jia, Q., Meng, T., Chow, V.T.K., and Kwang, J. (2014). A novel universal neutralizing monoclonal antibody against enterovirus 71 that targets the highly conserved "Knob" region of VP3 protein. PLoS Negl Trop Dis 8, e2895.

Ku, Z., Ye, X., Shi, J., Wang, X., Liu, Q., and Huang, Z. (2015). Single neutralizing monoclonal antibodies targeting the VP1 GH loop of enterovirus 71 inhibit both virus attachment and internalization during viral entry. J Virol 89, 12084–12095.

Lee, H., Cifuente, J.O., Ashley, R.E., Conway, J.F., Makhov, A.M., Tano, Y., Shimizu, H., Nishimura, Y., and Hafenstein, S. (2013). A strain-specific epitope of enterovirus 71 identified by cryo-electron microscopy of the complex with Fab from neutralizing antibody. J Virol 87, 11363–11370.

Li, X., Mooney, P., Zheng, S., Booth, C.R., Braunfeld, M.B., Gubbens, S., Agard, D.A., and Cheng, Y. (2013). Electron counting and beam-induced motion correction enable near-atomic-resolution single-particle cryo-EM. Nat Methods 10, 584–590.

Nhan, L.N.T., Hong, N.T.T., Nhu, L.N.T., Nguyet, L.A., Ny, N.T.H., Thanh, T.T., Han, D.D.K., Van, H.M.T., Thwaites, C.L., Hien, T.T., et al. (2018). Severe enterovirus A71 associated hand, foot and mouth disease, Vietnam, 2018: preliminary report of an impending outbreak. Eurosurveillance 23, 1800590.

Nishimura, Y., Wakita, T., and Shimizu, H. (2010). Tyrosine sulfation of the amino terminus of PSGL-1 is critical for enterovirus 71 infection. PLoS Pathog 6, e1001174.

Nishimura, Y., Lee, H., Hafenstein, S., Kataoka, C., Wakita, T., Bergelson, J.M., and Shimizu, H. (2013). Enterovirus 71 binding to PSGL-1 on leukocytes: VP1-145 acts as a molecular switch to control receptor interaction. PLoS Pathog 9, e1003511.

Nishimura, Y., Shimojima, M., Tano, Y., Miyamura, T., Wakita, T., and

Shimizu, H. (2009). Human P-selectin glycoprotein ligand-1 is a functional receptor for enterovirus 71. Nat Med 15, 794–797.

Oberste, M.S., Maher, K., Kilpatrick, D.R., and Pallansch, M.A. (1999). Molecular evolution of the human enteroviruses: correlation of serotype with VP1 sequence and application to picornavirus classification. J Virol 73, 1941–1948.

Ooi, M.H., Wong, S.C., Lewthwaite, P., Cardosa, M.J., and Solomon, T. (2010). Clinical features, diagnosis, and management of enterovirus 71. Lancet Neurol 9, 1097–1105.

Plevka, P., Perera, R., Cardosa, J., Kuhn, R.J., and Rossmann, M.G. (2012). Crystal structure of human enterovirus 71. Science 336, 1274.

Rader, C., Popkov, M., Neves, J.A., and Barbas, C.F. 3rd (2002). Integrin αvβ3-targeted therapy for Kaposi's sarcoma with an *in vitro*-evolved antibody. FASEB J 16, 2000–2002.

Ranganathan, S., Singh, S., Poh, C.L., and Chow, V.T. (2002). The hand, foot and mouth disease virus capsid: sequence analysis and prediction of antigenic sites from homology modelling. Appl Bioinformatics 1, 43–52.

Robbiani, D.F., Bozzacco, L., Keeffe, J.R., Khouri, R., Olsen, P.C., Gazumyan, A., Schaefer-Babajew, D., Avila-Rios, S., Nogueira, L., Patel, R., et al. (2017). Recurrent potent human neutralizing antibodies to Zika virus in Brazil and Mexico. Cell 169, 597–609.e11.

Rohou, A., and Grigorieff, N. (2015). CTFFIND4: fast and accurate defocus estimation from electron micrographs. J Struct Biol 192, 216–221.

Scheres, S.H.W. (2012). RELION: implementation of a Bayesian approach to cryo-EM structure determination. J Struct Biol 180, 519–530.

Schmidt, N.J., Lennette, E.H., and Ho, H.H. (1974). An apparently new enterovirus isolated from patients with disease of the central nervous system. J Infect Dis 129, 304–309.

Shingler, K.L., Cifuente, J.O., Ashley, R.E., Makhov, A.M., Conway, J.F., and Hafenstein, S. (2015). The enterovirus 71 procapsid binds neutralizing antibodies and rescues virus infection *in vitro*. J Virol 89, 1900–1908.

Tan, C.W., Poh, C.L., Sam, I.C., and Chan, Y.F. (2012). Enterovirus 71 uses cell surface heparan sulfate glycosaminoglycan as an attachment receptor. J Virol 87, 611–620.

Tang, G., Peng, L., Baldwin, P.R., Mann, D.S., Jiang, W., Rees, I., and Ludtke, S.J. (2007). EMAN2: an extensible image processing suite for electron microscopy. J Struct Biol 157, 38–46.

Wec, A.Z., Bornholdt, Z.A., He, S., Herbert, A.S., Goodwin, E., Wirchnianski, A.S., Gunn, B.M., Zhang, Z., Zhu, W., Liu, G., et al. (2019). Development of a human antibody cocktail that deploys multiple functions to confer pan-ebolavirus protection. Cell Host Microbe 25, 39–48.e5.

Yamayoshi, S., Yamashita, Y., Li, J., Hanagata, N., Minowa, T., Takemura, T., and Koike, S. (2009). Scavenger receptor B2 is a cellular receptor for enterovirus 71. Nat Med 15, 798–801.

Ye, X., Fan, C., Ku, Z., Zuo, T., Kong, L., Zhang, C., Shi, J., Liu, Q., Chen, T., Zhang, Y., et al. (2016). Structural basis for recognition of human enterovirus 71 by a bivalent broadly neutralizing monoclonal antibody. PLoS Pathog 12, e1005454.

Zost, S.J., Gilchuk, P., Case, J.B., Binshtein, E., Chen, R.E., Nkolola, J.P., Schäfer, A., Reidy, J.X., Trivette, A., Nargi, R.S., et al. (2020). Potently neutralizing and protective human antibodies against SARS-CoV-2. Nature 584, 443–449.

SUPPORTING INFORMATION

The supporting information is available online at https://doi.org/10.1007/s11427-021-2095-0. The supporting materials are published as submitted, without typesetting or editing. The responsibility for scientific accuracy and content remains entirely with the authors.